Journal of Environmental Radioactivity 142 (2015) 78–86

Contents lists available at ScienceDirect

Journal of Environmental Radioactivity

journal homepage: www.elsevier.com/locate/jenvrad

Ensemble-based simultaneous emission estimates and improved forecast of radioactive pollution from nuclear power plant accidents: application to ETEX tracer experiment

X.L. Zhang [a, b, *], Q.B. Li [b], G.F. Su [a], M.Q. Yuan [c]

[a] Institute of Public Safety Research, Department of Engineering Physics, Tsinghua University, Beijing, PR China
[b] Department of Atmospheric and Oceanic Sciences, University of California, Los Angeles, CA, USA
[c] School of Mechatronics Engineering, Beijing Institute of Technology, Beijing, PR China

ARTICLE INFO

Article history:
Received 21 September 2014
Received in revised form
10 January 2015
Accepted 14 January 2015
Available online 31 January 2015

Keywords:
Augmented ensemble Kalman filter
Emission estimate
Improve dispersion forecast
European Tracer Experiment
Nuclear power plant accident

ABSTRACT

The accidental release of radioactive materials from nuclear power plant leads to radioactive pollution. We apply an augmented ensemble Kalman filter (EnKF) with a chemical transport model to jointly estimate the emissions of Perfluoromethylcyclohexane (PMCH), a tracer substitute for radionuclides, from a point source during the European Tracer Experiment, and to improve the forecast of its dispersion downwind. We perturb wind fields to account for meteorological uncertainties. We expand the state vector of PMCH concentrations through continuously adding an *a priori* emission rate for each succeeding assimilation cycle. We adopt a time-correlated red noise to simulate the temporal emission fluctuation. The improved EnKF system rapidly updates (and reduces) the excessively large initial first-guess emissions, thereby significantly improves subsequent forecasts ($r = 0.83$, $p < 0.001$). It retrieves 94% of the total PMCH released and substantially reduces transport error (>80% average reduction of the normalized mean square error).

1. Introduction

During nuclear power plant accidents, the release of radioactive materials in the atmosphere leads to radioactive pollution. Near real-time information of radioactive material distribution is essential for doses estimation and in such way important for decision makers for planning accurate countermeasures like sheltering, evacuation and iodine-prophylaxis (Hiemstra et al., 2011). As a result, atmospheric dispersion models become critical and indispensable tools for nuclear power plant accident management (Benamrane et al., 2013; Connan et al., 2013). Dispersion models are also essential for assessing the external and internal radiological doses (Yoshida and Kanda, 2012). The largest source of uncertainties in the model predictions is the emission of radioactive materials (Stohl et al., 2012; Yasunari et al., 2011), which is usually unavailable, especially in the critical early stages of a nuclear power plant accident. In the Fukushima Daiichi power plant accident, for example, the damages caused by earthquake and the ensuing tsunami rendered the backup power system inoperative, and consequently there was no information of radioactive material release from the monitoring system (Chino et al., 2011). Adding to the myriad challenges for accurate model forecasts are large uncertainties of meteorological fields used in the forecast models (Jones, 2011). It is known the uncertainties in meteorological fields dominate the total transport error (Bei et al., 2012; Liu et al., 2011). The predictive capability of any dispersion model is severely limited by these aforementioned uncertainties.

Several studies have attempted to reconstruct the emissions of radionuclides from the Fukushima accident using observational datasets and chemical transport models (e.g., Ten Hoeve and Jacobson, 2012 and references therein). Chino et al. (2011), for instance, rescaled emissions of radionuclides based on comparisons of model predictions versus observations. More sophisticated inverse modeling methods were also used to reconstruct the emissions (e.g., Saunier et al., 2013; Stohl et al., 2012; Eslinger et al., 2014; Winiarek et al., 2012, 2014). These studies have offered valuable information for the accurate assessment of the environmental and healthy impacts of the accident (Ten Hoeve and

* Corresponding author. Institute of Public Safety Research, Department of Engineering Physics, Tsinghua University, Beijing 100084, PR China. Tel.: +86 10 62792894; fax: +86 10 62792863.
E-mail address: zhangxiaole10@mails.tsinghua.edu.cn (X.L. Zhang).

http://dx.doi.org/10.1016/j.jenvrad.2015.01.013
0265-931X/

Jacobson, 2012). In these inversion studies, the state vectors include only radionuclide emission rates and the simulations were conducted in a deterministic way. Thus it is difficult to take into account the uncertainties in the meteorological data used to drive their models. Additionally, the considerable time delay inherent in these studies makes it impractical for nuclear power plant emergency management.

The sequential assimilation method of ensemble Kalman filter (EnKF) (Evensen, 1994) is a powerful alternative for nuclear power plant emergency management. It has such advantages as efficient on-line calibration, relatively straightforward implementation and superior scalability for parallel computing. Furthermore, EnKF can simultaneously account for the various uncertainties in both emissions and meteorological data through the augmentation of the state vector, and simultaneously optimize parameters such as emissions in addition to the usual model state (Hu et al., 2010). Such augmentation has been applied in climate modeling (Annan et al., 2005), regional weather forecast (Hu et al., 2010), and carbon cycle (e.g., Kang et al., 2011; Miyazaki et al., 2011). Tang et al. (2011, 2013) has applied the augmented EnFK to simultaneously adjust the initial conditions and emissions of ozone and CO over Beijing and its surrounding areas. However, different from the air quality studies, where a lot of a *priori* knowledge (e.g., emission inventory) is available in literature, scarce (hence uncertain) *a priori* knowledge of accidental release is available, and order of magnitude discrepancy can exist between the first-guess and the actual emissions. And it is nearly impossible to directly validate the inversed emissions of common pollutants against the "actual" emissions. Zheng et al. (2007, 2009, 2010) has applied similar methodology, using the Monte Carlo dispersion model combined with EnKF to reconstruct the source release rate for short range dispersion. We have also developed a modified EnKF method in conjunction with a Lagrangian puff-model to simultaneously improve the model prediction and reconstruct the source terms (Zhang et al., 2013, 2014). However, these studies are only applicable for short range (usually under about 50 km) due to the limitation of the Lagrangian dispersion model. To the best of our knowledge, the approach has not been applied in studying accidental releases from nuclear power plants at the continental scale. In addition, it is imperative that the quality of the retrieved emissions of radioactive materials and improvements to model forecasts are thoroughly validated with observations.

The goal of this study is twofold. We seek to simultaneously estimate (and reconstruct) the emissions of radioactive materials from nuclear power plant accidents and to improve the dispersion forecast. We propose an innovative strategy for retrieving the emissions (with temporal resolution) despite scarce (hence uncertain) *a priori* knowledge of the emissions. Specifically, we apply an ensemble Kalman filter (EnKF) (Evensen, 1994) with an augmented dynamic state vector to simulate the emissions and subsequent dispersion of the released materials. In addition, we use perturbed wind fields to account for the uncertainties of meteorological data. We demonstrate and evaluate the method with the first European Tracer Experiment (ETEX-1) (Van dop et al., 1998), where Perfluoromethylcyclohexane (PMCH) was released as a tracer substituting for radioactive materials. Sensitivity tests are conducted to investigate the influence of different factors on the performance of the EnKF scheme.

2. Material and methods

2.1. Experiment and framework of modeling description

The goal of ETEX was to test the reaction, communications, and modeling capabilities of the European Union member countries in case of a nuclear emergency similar to the Chernobyl accident (Girardi et al., 1998). The European Commission, the World Meteorological Organization, the International Atomic Energy Agency and the U.S. Department of Energy together sponsored the experiment. It provides a unique dataset from a controlled point source release and an extensive monitoring surface network across Europe. The dataset is usually used to validate the newly developed data assimilation scheme or inverse method (e.g., Issartel and Baverel, 2003; Bocquet, 2007). We use the data of the first experiment ETEX-1 in this study. PMCH was released at Monterfil (48°03′30″N, 2°00′30″W), Brittany, France. PMCH is an inert gas, insoluble in water hence negligible wet (and dry) deposition. It has a half-life time of ~100 years. Perfluoromethylcyclohexane can be detected at extremely low concentrations, so making it ideal as a tracer. The release started at 16:00 UTC on October 23, 1994, and lasted 11 h and 50 min. A total of 340 kg PMCH was released at an average flow of 7.98 g s^{-1}. Air samples were taken at 168 stations up to 90 h after the initial release. The average distance between any two neighboring stations is ~80 km. There are 162 stations in the domain used here as shown in Fig. 1 and we use the data from these stations. The measurements are surface PMCH concentration reported every 3 h. The measurement resolution is 0.01 ng m^{-3}.

We conduct dispersion simulations of PMCH during the entirety of ETEX using the chemistry-transport model (CTM) POLAIR 3D (version 1.8.1), an Eulerian model of the POLYPHEMUS platform (Mallet et al., 2007). The domain plot is shown in Fig. 1. The horizontal resolution is 0.2° and there are nine vertical levels from the surface to 3184 m altitude for a total of 190 (longitude) × 98 (latitude) × 9 (altitude) grid points. Vertical turbulent diffusion is computed following Louis (1979). Except for the lower boundary condition at the surface, all other boundary conditions are null, following Winiarek et al. (2012). Meteorological data is from the Weather Research and Forecasting (WRF, version 3.1) (Skamarock et al., 2008), with a 20 km horizontal resolution (226 × 121 grid points) and 28 vertical layers. We initialize WRF simulation with NCEP/NCAR Reanalysis 1 data (Kalnay et al., 1996). The WRF simulation starts at 00:00 UTC, October 23, which is 16 h before the initial release of PMCH and lasts through 00:00 UTC, October 28, whereas the POLAIR 3D simulations start at the initial release time and last through 23:30 UTC, October 27. A 2-min time-step is used for both WRF and POLAIR 3D simulations. We conduct two WRF-POLAIR 3D simulations – one assimilates PMCH observations via EnKF with an unknown and uncertain initial PMCH emission rate, as discussed in Section 3, whereas the other is free running (i.e., without assimilation) but uses the actual (known) PMCH emission rates.

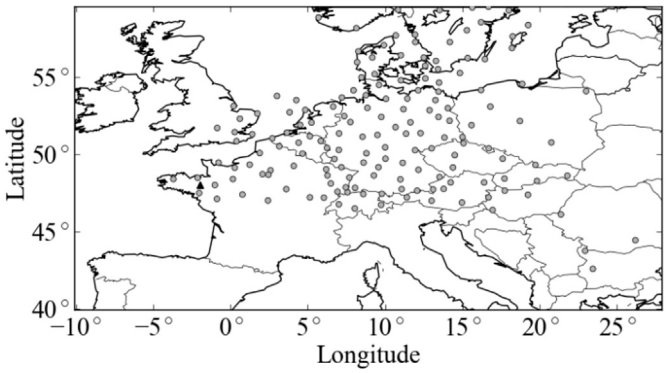

Fig. 1. The WRF-POLAIR model domain, PMCH release point (black triangle), and surface PMCH measurement network (gray dots, 162 stations).

2.2. The ensemble Kalman filter (EnKF)

The ensemble Kalman filter (EnKF) (Evensen, 1994) has been increasingly used in geosciences (Evensen, 2003). Ensemble Kalman filter (EnKF) is a sequential data assimilation method, which is used recursively to produce a statistically optimal estimate of the underlying system state by merging the model prediction and the current observations. Different from the original Kalman filter, which is only applicable to linear system model, the EnKF initializes an ensemble of forecast models, each of which represents a possible state of the system and the error statistics are predicted using the collection of model states. The ensemble state vectors constitute the state matrix:

$$\boldsymbol{X} = (x_1 \;\; x_2 \;\; \ldots \;\; x_N) \in \mathbf{R}^{n_s \times N} \tag{1}$$

where $\boldsymbol{x}$ is the state vector of the atmospheric dispersion system, the subscript i ($i = 1, 2, \ldots, N$) denotes the individual state vector of the ensemble, n_s is the length of the state vector and N denotes the size of the ensemble.

We use here the EnKF module of Mallet et al. (2007) with updates. Specifically, we expand the usual state vector, which consists of tracer concentrations in a CTM, to include emission rate, as discussed below. We use an ensemble size of 30. During the ETEX experiment, the first set of measurements was reported 2 h after the initial release, so the assimilation starts at that time and continues every 3 h thereafter. We assimilate the PMCH observations (3-h averages) by updating 3-h averaged model states of the ensemble and leaving the deviations from the time averages unchanged, following the approach of Dirren and Hakim (2005) for the assimilation of time-averaged observations. After the assimilation cycle, the deviations from the time averages are added back to the updated 3-h averaged model states, and the forecasts for the next 3 h start from the new model states. The ensemble mean of the updated 3-h averaged model states is referred to as "assimilation analysis" hereafter. The observation errors are set as 20% of the observed values (Straume et al., 1998) and are assumed to be spatiotemporally uncorrelated.

We perturb wind and vertical eddy diffusivity to simulate the uncertainty in the meteorological data and turbulent mixing. Specifically, we rescale the original winds from WRF to generate an ensemble of perturbed wind fields. The scaling factors are 0.5–1.5, uniform for each perturbation but varies from one perturbation to another. We choose the range because the majority of WRF wind forecasts are within a factor of two of the observations during ETEX (Stohl and Koffi, 1998). Likewise, we perturb vertical eddy diffusivity coefficients with factors that are uniformly distributed between 0.5 and 3.0. We use the relatively large range because of the typically large uncertainty associated with eddy diffusivity parameterizations (Kumar and Sharan, 2012). At this stage, we have not yet used the forecasts from real ensemble prediction system (EPS). We note that discrepancies will exist between the perturbed ensemble and the ensemble forecasts from EPS system, and the performance can be sensitive to the ensemble of meteorological data, so the sensitivity tests will be conducted and discussed in Section 3.4.

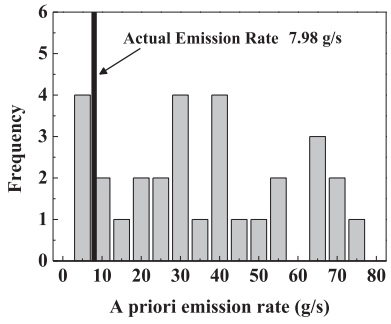

Fig. 2. The actual and *a priori* emission rate ensemble used.

We set the initial emission rate as uniformly distributed between 0 and 100 g s^{-1} – any value between 0 and 100 g s^{-1} is equally probable of being the actual emission rate, whereas the actual rate is 7.98 g s^{-1}. The rather large upper limit is based upon the inventory of the hazardous materials in the reactor units of an average-size nuclear power plant, which is usually known. We then draw 30 samples from the uniform distribution to generate an ensemble of (initial) emission rates. Fig. 2 shows the ensemble alongside the actual rate (black bar).

2.3. State vector augmentation

We expand the state vector to include not only the usual state variables of PMCH concentrations but also PMCH emission rates as follows,

$$\boldsymbol{x} = (c_1, \;\; c_2, \;\; \cdots \;\; c_{m\times n\times k}, \;\; Q_1, \;\; Q_2, \;\; \cdots \;\; Q_h)^{\mathrm{T}} \in \mathbf{R}^{m\times n\times k+h} \tag{2}$$

where c_i is the PMCH concentration at the i-th grid point, m, n and k the horizontal and vertical dimensions of the assimilation system, Q_i the emission rate during the i-th assimilation step, and h the number of discrete emission periods. The simulation is discretized into 3-h time periods to better represent the temporal evolution of the emission rate, which is assumed to be constant during each (3-h) time period. The emission and data assimilation frequencies are both 3-hourly, the same as the observation frequency. At the end of each 3-h time period, an *a priori* emission rate for the next period is added to the state vector, thereby increasing the dimension of the state vector and resulting in a dynamically expanding state vector over time. An obvious and defining advantage of our augmentation approach is that the emission trajectory is tracked and preserved in the state vector, thereby allowing the emission rate to be continuously updated by the EnKF. Theoretically, the emission rate will converge apace toward the actual value after the first few steps of assimilation.

2.4. Simultaneous update of concentration and emission rate

We compute the *a priori* emission rate for the next time period as the mean of the updated emission rate ensemble from the current time period:

$$Q_h^b = \sum_{i=1}^{N} Q_{h-1}^a(i)/N \tag{3}$$

where the superscript a indicates the analysis results from the assimilation, i the index in the ensemble, and N the ensemble size. We then generate a new emission rate ensemble for the next 3-h emission time period by adding random noise to the *a priori* estimate Q_h^b following Tang et al. (2011),

$$Q_h^f(i) = Q_h^b + \delta Q_h^b(i), \;\; i = 1, 2, \ldots, N \tag{4}$$

where $\delta Q_h^b(i)$ is the random noise. We assume that the emission is persistent within each 3-h time step, a reasonable assumption justified by the relatively short time frame. Assuming that the emission rate does not fluctuate dramatically over time, we then

adopt a time-correlated red noise to simulate the temporal evolution of the emission rate perturbation (Hartmann, 2014):

$$\delta Q_h^b(i) = \alpha \delta Q_{h-1}^a(i) + \sqrt{1-\alpha^2} w_{h-1}(i)\sigma, \quad i = 1, 2, \ldots, N \tag{5}$$

where $\delta Q_{h-1}^a(i)$ is the deviation of the i-th analysis emission rate from the ensemble mean, α (between 0 and 1) the degree to which the influence ("memory") of the previous state is retained, $w_{h-1}(i)$ a random number following normal distribution $N(0, 1)$, and σ the standard deviation calculated from the current analysis emission rate ensemble Q_{h-1}^a. We use here $\alpha = 0.5$ to provide reasonable sensitivity to both constant and rapidly changing emissions. The emission rate tends to converge to the actual value, and the standard deviation of the ensemble decreases. A small deviation sometimes leads to "filter divergence" in EnKF (Ehrendorfer, 2007), whereby the emission rates do not respond to the assimilation of new observations anymore and the ensemble mean deviates from the actual value. To avoid such divergence, we impose a minimum standard deviation of 10% of the ensemble mean as follows,

$$\sigma = \max\left(\sigma(Q_{h-1}^a),\ 0.1 \times \overline{Q_{h-1}^a}\right) \tag{6}$$

Ten percent is sufficiently large to instigate the correction of the ensemble if the *a priori* value differs substantially from the actual rate. Yet it does not contaminate the estimate because its rapid dissipation.

3. Results and discussions

3.1. Assimilation quality

We first compare the analysis PMCH concentrations against the observations used in the assimilations as a "sanity check". Here we use four statistical metrics to quantify the performance of the assimilation: fractional bias (FB), normalized mean square error (NMSE), fraction of the predictions within a factor three of observations (FAC3) and correlation coefficient (r), following (Korsakissok and Mallet, 2009). FB and NMSE are defined as:

$$\mathrm{FB} = \left(\overline{C}_{\mathrm{obs}} - \overline{C}_{\mathrm{assim}}\right) / \left(0.5\left(\overline{C}_{\mathrm{obs}} + \overline{C}_{\mathrm{assim}}\right)\right) \tag{7}$$

$$\mathrm{NMSE} = \overline{(C_{\mathrm{obs}} - C_{\mathrm{assim}})^2} \Big/ \left(\overline{C}_{\mathrm{obs}} \overline{C}_{\mathrm{assim}}\right) \tag{8}$$

where C_{obs} is the observed PMCH concentration and C_{assim} is the PMCH concentration from the EnKF data assimilation analysis. The same metrics are also applied to the model forecast without data assimilation.

The EnKF scheme can effectively assimilate the observations. Fig. 3 is a scatter plot of model simulated PMCH surface concentrations, with and without data assimilation, against the observations. Since the measurement resolution is 0.01 ng m^{-3}, the model results are rounded off to the nearest 0.01 ng m^{-3}. We only include the nonzero observations in the comparison. Relative to the observations, the forecast without assimilation shows a substantial bias (FB = −105%), a large error (NMSE = 50.74), and a weak correlation (r = 0.64), with only 48% of the forecast PMCH concentrations within a factor of three of the observations, despite using the actual emission rates. In contrast, the EnKF assimilation substantially reduces the bias (FB = 29%) and error (NMSE = 2.22) and increases the correlation (r = 0.83, $p < 0.001$), with 63% of the analysis PMCH concentrations within a factor three of the observations.

Fig. 4 shows the 3-h averaged PMCH surface concentrations from the model forecast without assimilation (but with the actual emission rates) and from the EnKF assimilation analysis (with uncertain emission rates) during hours 45–47 (left column) and hours 69–71 (right column). There is a small yet appreciable performance improvement from the assimilation analysis during the first time period. For the latter time period, the assimilation analysis shows a significant improvement. The concentrations are dramatically overestimated by the model forecast without assimilation (FB = 114%, NMSE = 11.66). The forecast and the observations become anti-correlated (r = −0.19). The EnKF assimilation, in contrast, greatly reduces the bias (FB = −10%), increases the correlation between the analysis and observed PMCH (r = 0.52), and lowers the error (NMSE = 0.96). The differing distributions of model predicted and observed plumes indicate that meteorological uncertainty is a significant part of the transport errors (Bei et al., 2012; Liu et al., 2011). The model forecast without assimilation deteriorates in accuracy with increasing forecast time because of the accumulation of the transport errors. Contrastingly, the EnKF assimilation effectively and efficiently 'calibrates' the transport error.

3.2. Emission rate reconstruction

Fig. 5 (left panel) shows the actual, *a priori* and *a posteriori* PMCH emission rates. The *a priori* rate is several times higher than the actual rate during the initial four assimilation cycles (up to hour 11 since the initial release). This is directly because of the rather large initial guess of *a priori* rate used at the start of the EnKF assimilation. The assimilation effectively updates and adjusts the *a priori*

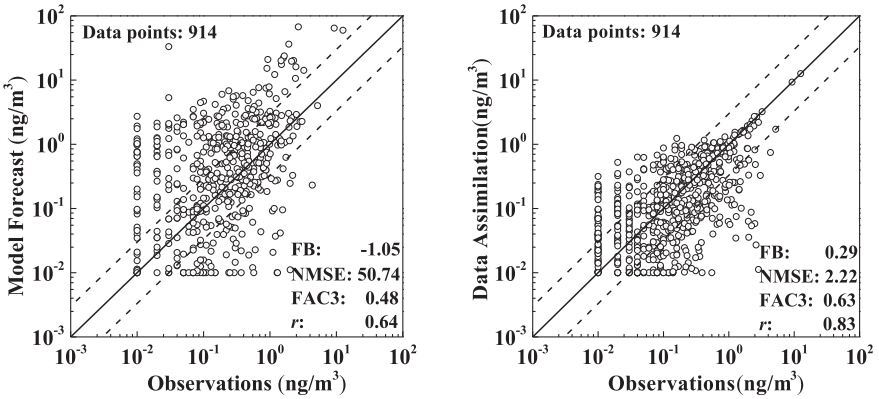

Fig. 3. Scatter plots of observed versus model forecasted surface PMCH concentration: (left) model forecast with the actual emissions but without assimilation; (right) model forecast with assimilation and with uncertain emissions. See text for details. Values are 3-h averages. Dashed lines are 1:3 (or 3:1) ratio lines.

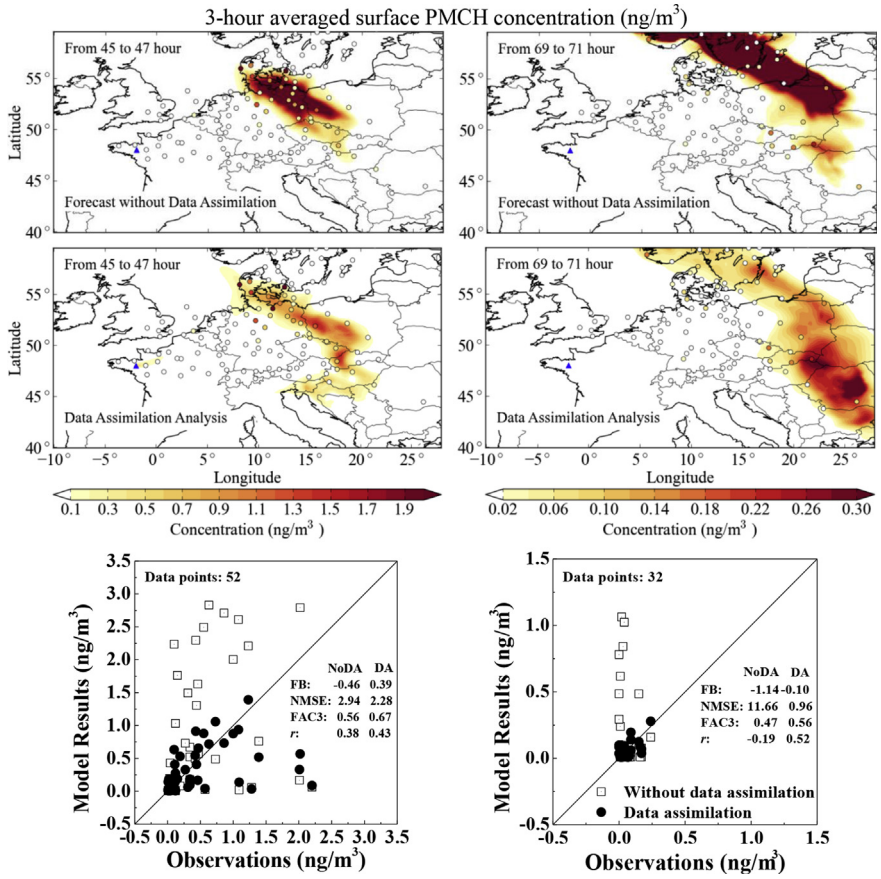

Fig. 4. (Top and middle panels) Model forecasted surface PMCH concentrations during hours 45–47 (left panels) and 69–71 (right panels): (top panels) forecast with the actual known emissions but without assimilation ("NoDA"); (middle panels) forecast with assimilation and unknown and uncertain emissions ("DA"). Observation (circles) are color-coded. Different concentration scales are used for the two time periods here. (Bottom panels) scatter plots of model forecasted versus observed surface PMCH concentrations: (left) during hours 45–47; (right) during hours 69–71. See text for details. Values are 3-h averages. (For interpretation of the references to color in this figure legend, the reader is referred to the web version of this article.)

emission rate (via Eq. (4)), which rapidly decreases and approaches the actual rate. The ensemble *a posteriori* emission rates at hour 15 fall into the range 1.8–10.0 g s^{-1} (mean = 5.9 g s^{-1}, median = 6.4 g s^{-1}), encompassing the actual rate. The emission uncertainty is also reduced by five folds.

The *a posteriori* temporal evolution of the emission rate retrieved at hour 90 (since the initial release) is shown (as bars) in Fig. 5 (left panel). All available observations have been assimilated by that time. The *a posteriori* rates are closer to the actual values compared with the *a priori* rates. The EnKF assimilation captures the overall temporal evolution of the emissions: large early on and no emissions afterward. The *a posteriori* emission rates at hours 3–5 (3 h from 18:00 UTC to 21:00 UTC, October 23) and 12–14 (3 h from 3:00 UTC to 6:00 UTC, October 24) are 16% and 25% higher than the corresponding rates in the experiment. The retrieved emission rate converges to 10^{-2} g s^{-1} after the first five assimilation steps. The biases for the first, third and fourth periods are large. For the first period (hours 1–2), the emission rate is overestimated threefold. For the third (hours 6–8) and fourth (hours 9–11) periods, the emission rates are underestimated. The overestimated

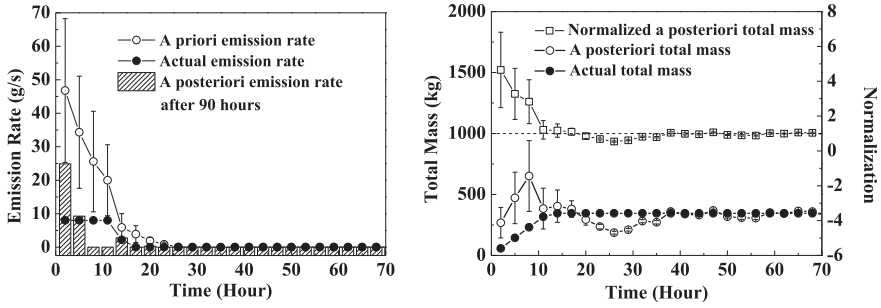

Fig. 5. (Left) The actual (solid circles), the *a priori* (open circles), and the *a posteriori* (shaded bars) emission rates –the latter is reconstructed 90 h after the initial release. Error bar indicates the standard deviation of the ensemble. Since the release only lasted for 50 min (from 3:00 UTC to 3:50 UTC, October 24) during the fifth period (hours 12–14), its "actual emission rate" is the averaged rate over the 3 h, which is 2.81 g s^{-1}. (Right) The actual total PMCH mass released, the *a posteriori* total PMCH mass summed over the model domain (Fig. 1) after each data assimilation point, and the normalized *a posteriori* total mass by the actual value.

part of the first period approximately fills the gaps between actual emission and estimation of the third and fourth periods. In the model, extra amount of material has been released into atmosphere due to the excessively large initial guess, so the model simulation are generally overestimated. The EnKF scheme attributes the overestimation of the model forecast to the errors of the initial emission rate, so it reduces the emission rates to decrease the surface concentration. But it cannot eliminate all the extra PMCH at once. As a result, the remaining extra PMCH plume around the source takes the place of succeeding emissions, and consequently suppresses the estimated emissions for subsequent periods, resulting in large bias.

The reconstructed total emission of PMCH is much more accurate. The actual release is 340 kg in total. The EnKF assimilation is able to recover 94% of the total emission, a substantial improvement over the total emissions retrieved by Bocquet (2007) (85%) and by Seibert (2001) (61%). The temporal evolution of the total mass of PMCH summed over the computational domain is shown in Fig. 5 (right panel). The emissions begin exiting the domain 70 h after the initial release. The *a posteriori* total mass of PMCH is normalized by the actual value (open squares in Fig. 5). Initially, the total mass is overestimated by a factor of 5. It takes about 35 h for the reconstructed total mass of PMCH to converge toward its actual value.

3.3. Forecast improvements

Here we appraise the forecast skill of the updated EnKF scheme, which assimilates the observations of PMCH surface concentration during ETEX and estimates and updates the (otherwise unknown and uncertain) emission rate of PMCH. Specifically, we compare and contrast the EnKF forecast with the forecast that uses the actual (known) emission rates of PMCH but does not assimilate any observations. Fig. 6 shows the time evolution of the correlation coefficient (r) and NMSE of the forecast PMCH concentrations versus the observations. Initially (hours 0–5) NMSE is considerably larger in the EnKF forecast than in the one without assimilation. That is because of the rather large initial guess of PMCH emission rate used in the assimilation. During hours 11–60, the two sets of NMSE become increasingly comparable (within 60%) as the EnKF forecast continuously updates the emission rate, effectively reduces the associated uncertainties, and consequently improves the forecast. From hour 60 onward, the forecast without assimilation

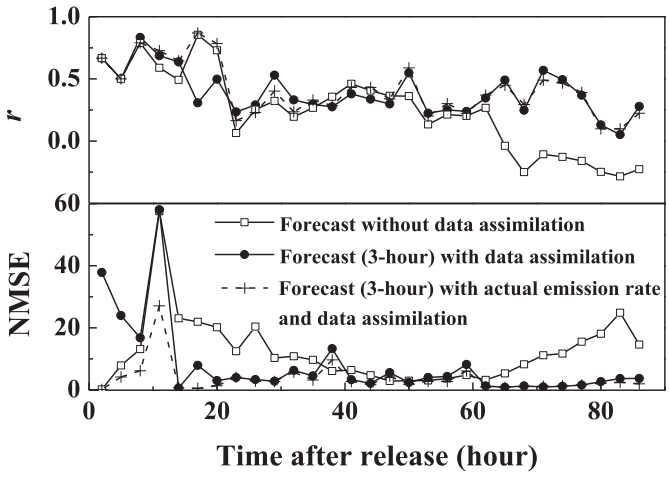

Fig. 6. Correlation coefficient (top) and normalized mean square error (bottom) between observed and forecasted (with and without assimilation) surface PMCH concentrations. Values are 3-h averages.

deteriorates in quality due to the accumulation of the transport errors, as evidenced in the sharply increasing NMSE (from 4.06 to 24.86) and rapidly decreasing correlation coefficient (from 0.35 to −0.28). In contrast, the EnKF forecast performs considerably better during hours 11–90 as evident in the relatively steady correlation coefficient (~0.40 on average) and small NMSE (3.70 on average, ~80% reduction relative to the initial values). These results are consistent with those in Fig. 4. The EnKF forecast quality suffers slightly around hour 80 because of the diminishing number of observations. Overall the EnKF forecast dramatically outperforms the forecast without assimilation.

We also conduct the forecast with data assimilation, and with the actual emission rate to investigate the pure effectiveness of data assimilation for meteorological data. The results are shown as cross-dash line in Fig. 6. During the first 20 h, the forecast with data assimilation and actual emission rate is better (~63% reduction in NMSE and ~35% improvement in correlation coefficient on average) than in the one with unknown emission rate. The differing performance indicates that during the first 20 h, the unknown emission rate has a substantial influence on the surface concentration, and the updated EnKF scheme simultaneously 'calibrates' the errors both in the emission rate and meteorological data. From hour 20 onward, the EnKF forecasts with and without the actual emission rate become comparable (within 19% in correlation coefficient and 20% in NMSE on average), which indicates that the influence of the unknown emission rate has decreased and the EnKF scheme mainly 'calibrates' the error in the meteorological data.

The NMSE in the forecast without data assimilation decreases from a high level early on, to a low level in the middle of the experiment. The substantial error during the first 20 h is mainly caused by the "false-diffusion" of the Eulerian approach used in our study. In Eulerian models, emissions from major point sources are usually assumed to mix immediately within a grid cell. The rapid mixing will cause relatively large error in the vicinity of the source, where plume does not expand to the size of the grid box (Korsakissok and Mallet, 2010). As a result, the forecast of Eulerian model without data assimilation has large errors during the first 20 h as shown in Fig. 6. The large overall NMSE (50.74) in Fig. 3 is mainly caused by the poor performance during the fourth period, when the NMSE amounts to about 60. The Lagrangian atmospheric dispersion model in (Davakis et al., 2007) provides a better representation of the near-source dispersion, and the overall value of NMSE without any data assimilation during the first 33 h after the release was about 15, which is much better than the overall NMSE (50.74) in our study. Korsakissok and Mallet (2010) evaluated the plume-in-grid method with ETEX I. The Eulerian model POLAIR 3D in (Korsakissok and Mallet, 2010) gave a large error (NMSE = 47.7) at station F21, but it decreased to 8.5 when the Eulerian model was coupling with a lagrangian sub-grid model in the near source area. The "false-diffusion" problem is substantially alleviated as evident in the small NMSE of the 3-h forecast with data assimilation and actual emission rate during the first 20 h.

3.4. Sensitivity tests

The performance of the updated EnKF scheme depends on several factors, such as the first-guess emissions and the ensemble of the meteorological data. In order to investigate the influence of these factors, sensitivity tests are conducted and summarized in Table 1. The experiment discussed in the previous sections is referred to as "Base-Test" hereafter.

The first sensitivity test ST01 is to investigate the influence of the first-guess emissions. In the Base-Test, the initial emission rate is set as uniformly distributed between 0 and 100 g s^{-1}, and the actual rate (7.98 g s^{-1}) locates within the range. In ST01, the initial

emission rate is set as uniformly distributed between 0 and 1 g s^{-1}, which is substantially underestimated (with a mean of 0.5 g s^{-1}, only 6.3% of the actual rate), and the actual rate is outside the range of the first-guess. The main results are shown in Table 2. The updated EnKF scheme also successfully retrieves 94% of the total emission. Table 2 also shows the statistical metrics of the assimilation analysis. The metrics are close to those in the Base-Test, which shows the scheme successfully assimilates the observations. This result suggests that the performance of the updated EnKF scheme is not sensitive to the first-guess emissions, and the robustness is beneficial for practical applications.

In the Base-Test, We perturb wind to simulate the uncertainty in the meteorological data. The second test ST02 is conducted to evaluate the sensitivity of the data assimilation scheme to the perturbation added into the wind field. In ST02, we use a different kind of distribution, lognormal distribution (0, 0.5), to generate the rescaling factors. The comparison of the two different distributions is shown in Fig. 7. The rescaling factors only distribute between 0.5 and 1.5 in the Base-Test, but they distribute between 0 and 4 in ST02. The broader distribution indicates larger uncertainties are introduced in the wind fields. The main results of ST02 are shown in Table 2. It shows that the total mass is overestimated by 22%. The bias is attributed to the large uncertainties in the wind fields, which leads to substantial uncertainties in the horizontal distribution of the PMCH plume. Some extra part of the plume cannot be effectively eliminated by the data assimilation due to the sparse observation network. As a result, the horizontal extent of the PMCH plume is generally larger than that in the Base-Test, consequently leading to the overestimation. However, considering the substantial overestimation of the first-guess emission, the results are still acceptable. The metrics show the observations have been effectively assimilated. The results indicate the updated EnKF scheme is moderately sensitive to the perturbation added into the wind field.

In the updated EnKF scheme, we adopt a time-correlated red noise to simulate the temporal evolution of the emission rate perturbation, and the parameter α is introduced in Eq. (5). ST03 is conducted to investigate the influence of the parameter. α is set as 0.1 in the sensitivity test. The reconstructed total emission of PMCH is slightly overestimated by 5%, and the metrics are also very close to those in the Base-Test. The results suggest that the performance of the data assimilation scheme is not sensitive to the new introduced parameter.

The fourth sensitivity test ST04 is to evaluate the effect of the meteorological uncertainty. The wind field is not perturbed, and only the uncertainties of the vertical eddy diffusivity coefficients are taken into account in the meteorological ensemble. The performance substantially deteriorates as shown in Table 2. It only retrieves 57% of the total released mass. The results are consistent with the findings by Jiang et al. (2011) and Tang et al. (2013), and it suggests that neglecting the uncertainties of the meteorological data can lead to bias in the emission estimations. The results of ST02 and ST04 indicate that the uncertainties in the meteorological field exert a relatively strong influence on the performance of the updated EnKF scheme.

Table 1
Sensitivity tests to investigate the sensitivity of the updated EnKF scheme to the different factors.

Tests	Sensitivity factors	Test setup
ST01	First-guess emissions	Uniformly distributed between 0 and 1 g s^{-1}
ST02	Wind field rescaling factors	Following lognormal distribution (0, 0.5)
ST03	Red noise parameter α	Set as 0.1
ST04	Wind field uncertainties	Removed
ST05	Number of the observations	Remove 15 (9.26%) stations

Table 2
Reconstructed total mass and statistical metrics of the assimilation analysis in the sensitivity tests. The retrieved percentages of the actual total mass are given in the brackets.

	Reconstructed total mass (kg)	FB	NMSE	FAC3	r
Base-Test	319.60 (94%)	0.29	2.22	0.63	0.83
ST01	321.39 (94%)	0.41	2.94	0.61	0.80
ST02	415.68 (122%)	0.19	2.03	0.64	0.82
ST03	353.64 (105%)	0.28	2.38	0.61	0.81
ST04	193.07 (57%)	0.41	3.14	0.56	0.79
ST05	369.05 (109%)	0.26	2.11	0.63	0.84

The sensitivity test ST05 is to investigate the influence of the number of the observations. We remove the observations at 15 stations (9.26% of the total stations, shown as red points in Fig. 8) from the data assimilation dataset, so the measurements from these stations will not be used in the data assimilation. The removed stations are referred to as “validation sites” hereafter. The reconstructed total emission of PMCH in ST05 is slightly overestimated by 9%, so the removal of the 15 stations only has limited impact on the performance. We also conduct independent comparisons with the measurements at the validation sites. The bottom panels of Fig. 8 are scatter plots of model simulated PMCH surface concentrations, with and without data assimilation, against the observations at the validation sites. The data assimilation scheme substantially reduces the fractional bias (from −110% to 6%) and the normalized mean square error (from 27.12 to 4.37). The fraction of forecasts within a factor three of observations is also improved by 7%. The correlation coefficient is slightly decreased by 0.01. In general, the updated EnKF scheme improves the overall forecast quality at the validation sites.

4. Summary and conclusions

We employed an Ensemble Kalman filter (EnKF) with the POLAIR 3D chemical transport model driven by WRF meteorological data to simultaneously estimate the emissions and to improve the dispersion forecast of Perfluoromethylcyclohexane (PMCH), a substitute tracer for radioactive materials during the European Tracer Experiment. We augmented the EnKF state vector (of concentrations) to include emission rates. The augmentation thus enabled at once the continuous optimization of PMCH emission rate including its temporal variation and the improved forecast of the downwind dispersion of PMCH. Meteorological uncertainty was simulated by perturbing the wind fields from WRF. The augmented EnKF, coupled with the WRF-POLAIR models, was then applied to assimilate time-averaged surface PMCH concentrations every 3 h.

The assimilation/inversion system initially overestimated the emission rate “three-fold” because of the excessively large initial

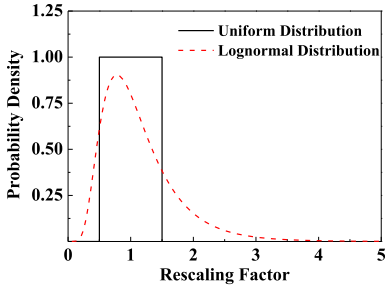

Fig. 7. Comparison of the two different probability density functions for wind rescaling factors: uniform distribution in the Base-Test, and lognormal distribution in ST02.

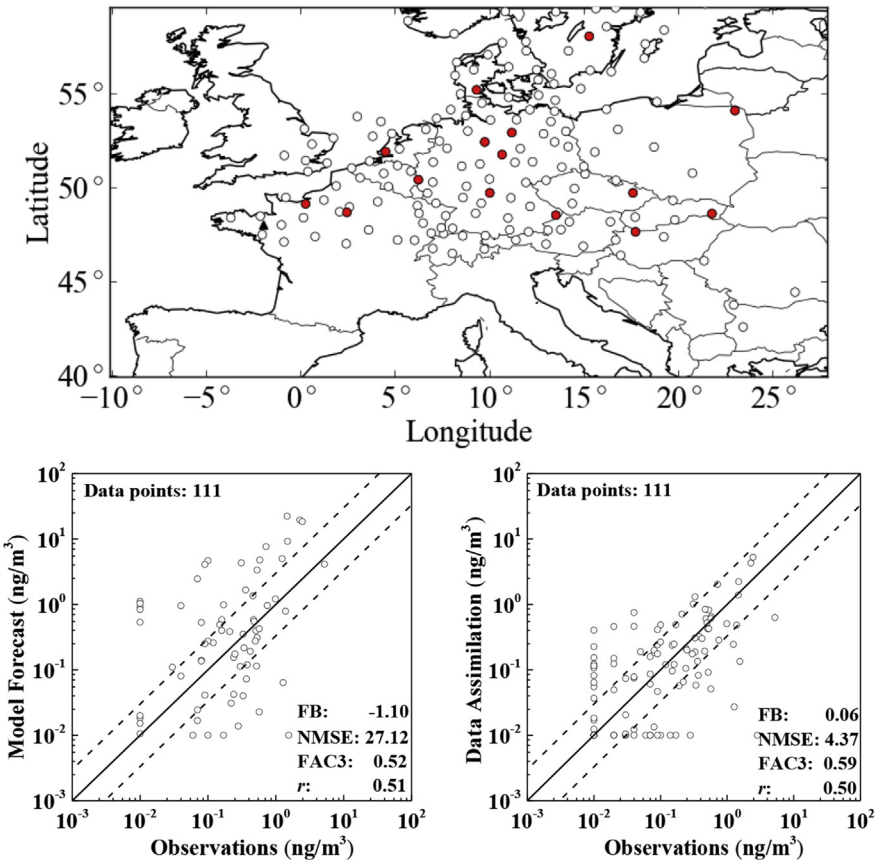

Fig. 8. (Top panel) Locations of the validation sites (red points). (Bottom panels) scatter plots of model forecasted versus observed surface PMCH concentrations at the validation sites: (left) forecast without assimilation; (right) forecast with assimilation. See text for details. Values are 3-h averages. (For interpretation of the references to color in this figure legend, the reader is referred to the web version of this article.)

guess but rapidly converged toward the actual rates. The system retrieved the total emissions of PMCH remarkably well, recovering ~94% of the actual total PMCH release, an improvement to previous studies. The influence of the overestimated initial emission rate on subsequent emission estimates and forecasts tapered rapidly during the first several hours. The assimilation/inversion system, initialized with unknown hence largely uncertain PMCH emission rates, significantly outperformed the free-running WRF-POLAIR models (with the actual, known PMCH emission rates) in predicting downwind surface PMCH concentrations. In particular, the system captured the shift of the PMCH plume from Northern to Eastern Europe toward the later part of the experiment. The sensitivity tests suggest that the updated EnKF scheme is not sensitive to the first-guess emissions and the parameter α introduced in the time-correlated red noise. But the uncertainties in the meteorological field exert a relatively strong influence on the performance.

The updated EnKF scheme is presently applicable for gaseous radionuclides, e.g., noble gas Xenon-133 and gaseous iodine. Ongoing research includes extending the scheme to particulate radionuclides (e.g., Cesium-137 and particulate iodine) and to other events where near-real-time emission estimates and forecasts are critical. The extended scheme can be validated with the data from the International Global Atmospheric Chemistry (IGAC) project, such as the Aerosol Characterization Experiments (ACEs) (Bates et al., 1998).

Acknowledgments

The data used in this study is from the dataset of European Tracer Experiment project http://rem.jrc.ec.europa.eu/etex/. We thank the support provided by the National High-Tech Research and Development Program of China (863 Program) (No. 2012AA050907).

References

Annan, J.D., Lunt, D.J., Hargreaves, J.C., Valdes, P.J., 2005. Parameter estimation in an atmospheric GCM using the Ensemble Kalman Filter. Nonlinear Process. Geophys. 12 (3), 363–371.

Bates, T.S., Huebert, B.J., Gras, J.L., Griffiths, F.B., Durkee, P.A., 1998. International global atmospheric chemistry (IGAC) Project's first aerosol characterization Experiment (ACE 1): overview. J. Geophys. Res. Atmos. 103 (D13), 16297–16318.

Bei, N., Li, G., Molina, L.T., 2012. Uncertainties in SOA simulations due to meteorological uncertainties in Mexico City during MILAGRO-2006 field campaign. Atmos. Chem. Phys. 12 (23), 11295–11308.

Benamrane, Y., Wybo, J.L., Armand, P., 2013. Chernobyl and Fukushima nuclear accidents: what has changed in the use of atmospheric dispersion modeling? J. Environ. Radioact. 126 (0), 239–252.

Bocquet, M., 2007. High-resolution reconstruction of a tracer dispersion event: application to ETEX. Q. J. Roy. Meteor. Soc. 133 (625), 1013–1026.

Chino, M., Nakayama, H., Nagai, H., Terada, H., Katata, G., Yamazawa, H., 2011. Preliminary estimation of release amounts of 131I and 137Cs accidentally discharged from the fukushima daiichi nuclear power plant into the atmosphere. J. Nucl. Sci. Technol. 48 (7), 1129–1134.

Connan, O., Smith, K., Organo, C., Solier, L., Maro, D., Hébert, D., 2013. Comparison of RIMPUFF, HYSPLIT, ADMS atmospheric dispersion model outputs, using emergency response procedures, with 85Kr measurements made in the vicinity of nuclear reprocessing plant. J. Environ. Radioact. 124 (0), 266–277.

Davakis, E., Andronopoulos, S., Kovalets, I., Gounaris, N., Bartzis, J.G., Nychas, S.G., 2007. Data assimilation in meteorological pre-processors: effects on atmospheric dispersion simulations. Atmos. Environ. 41 (14), 2917–2932.

Dirren, S., Hakim, G.J., 2005. Toward the assimilation of time-averaged observations. Geophys. Res. Lett. 32 (4), L04804.

Ehrendorfer, M., 2007. A review of issues in ensemble-based Kalman filtering. Meteorol. Z. 16 (6), 795–818.

Eslinger, P.W., et al., 2014. Source term estimation of radioxenon released from the Fukushima Dai-ichi nuclear reactors using measured air concentrations and atmospheric transport modeling. J. Environ. Radioact. 127 (0), 127–132.
Evensen, G., 1994. Sequential data assimilation with a nonlinear quasi-geostrophic model using monte-carlo methods to forecast error statistics. J. Geophys. Res.-Oceans 99 (C5), 10143–10162.
Evensen, G., 2003. The Ensemble Kalman Filter: theoretical formulation and practical implementation. Ocean Dyn. 53 (4), 343–367.
Girardi, F., Graziani, G., Van Velzen, D., Galmarini, S., Mosca, S., Bianconi, R., Bellasio, R., Klug, W., Fraser, G., 1998. ETEX – the European Tracer Experiment. EUR 18143 EN. Official Publications of the European Communities, Luxembourg, p. 108.
Hartmann, D., 2014. Objective Analysis: Section 6a Time (Or Space) Series Analysis. University of Washington, Seattle, Washington. Available at: http://www.atmos.washington.edu/~dennis/552_Notes_6a.pdf. unpublished manuscript.
Hiemstra, P.H., Karssenberg, D., Van Dijk, A., 2011. Assimilation of observations of radiation level into an atmospheric transport model: a case study with the particle filter and the ETEX tracer dataset. Atmos. Environ. 45 (34), 6149–6157.
Hu, X.M., Zhang, F., Nielsen-Gammon, J.W., 2010. Ensemble-based simultaneous state and parameter estimation for treatment of mesoscale model error: a real-data study. Geophys. Res. Lett. 37 (8), L08802.
Issartel, J.P., Baverel, J., 2003. Inverse transport for the verification of the Comprehensive Nuclear Test Ban Treaty. Atmos. Chem. Phys. 3 (3), 475–486.
Jiang, Z., Jones, D.B.A., Kopacz, M., Liu, J., Henze, D.K., Heald, C., 2011. Quantifying the impact of model errors on top-down estimates of carbon monoxide emissions using satellite observations. J. Geophys. Res. Atmos. 116 (D15), D15306.
Jones, A.R., 2011. Assessing meteorological uncertainties in dispersion forecasts using a NWP Ensemble Prediction System. Int. J. Environ. Pollut. 44 (1–4), 208–216.
Kalnay, E., et al., 1996. The NCEP/NCAR 40-Year reanalysis project. Bull. Am. Meteorol. Soc. 77 (3), 437–471.
Kang, J.-S., Kalnay, E., Liu, J., Fung, I., Miyoshi, T., Ide, K., 2011. "Variable localization" in an ensemble Kalman filter: application to the carbon cycle data assimilation. J. Geophys. Res. Atmos. 116 (D9), D09110.
Korsakissok, I., Mallet, V., 2009. Comparative study of Gaussian dispersion formulas within the Polyphemus platform: evaluation with Prairie Grass and Kincaid experiments. J. Appl. Meteorol. Climatol. 48 (12), 2459–2473.
Korsakissok, I., Mallet, V., 2010. Subgrid-scale treatment for major point sources in an Eulerian model: a sensitivity study on the European Tracer Experiment (ETEX) and Chernobyl cases. J. Geophys. Res. Atmos. 115 (D3), D03303.
Kumar, P., Sharan, M., 2012. Parameterization of the eddy diffusivity in a dispersion model over homogeneous terrain in the atmospheric boundary layer. Atmos. Res. 106 (0), 30–43.
Liu, J., Fung, I., Kalnay, E., Kang, J.-S., 2011. CO_2 transport uncertainties from the uncertainties in meteorological fields. Geophys. Res. Lett. 38 (12), L12808.
Louis, J.-F., 1979. A parametric model of vertical eddy fluxes in the atmosphere. Bound.-Layer Meteorol. 17 (2), 187–202.
Mallet, V., et al., 2007. Technical note: the air quality modeling system Polyphemus. Atmos. Chem. Phys. 7 (20), 5479–5487.
Miyazaki, K., Maki, T., Patra, P., Nakazawa, T., 2011. Assessing the impact of satellite, aircraft, and surface observations on CO_2 flux estimation using an ensemble-based 4-D data assimilation system. J. Geophys. Res. Atmos. 116.
Saunier, O., Mathieu, A., Didier, D., Tombette, M., Quelo, D., Winiarek, V., Bocquet, M., 2013. An inverse modeling method to assess the source term of the Fukushima Nuclear Power Plant accident using gamma dose rate observations. Atmos. Chem. Phys. 13 (22), 11403–11421.
Seibert, P., 2001. Inverse modelling with a lagrangian particle disperion model: application to Point releases over limited time intervals. In: Gryning, S.-E., Schiermeier, F. (Eds.), Air Pollution Modeling and its Application XIV. Springer, US, pp. 381–389.
Skamarock, W.C., Klemp, J.B., Dudhia, J., Gill, D.O., Barker, M., Duda, K.G., Huang, Y., Wang, W., Powers, J.G., 2008. A Description of the Advanced Research WRF Version 3Rep, pp. 1–113.
Stohl, A., Koffi, N.d.E., 1998. Evaluation of trajectories calculated from ecmwf data against constant volume balloon flights during etex. Atmos. Environ. 32 (24), 4151–4156.
Stohl, A., Seibert, P., Wotawa, G., Arnold, D., Burkhart, J.F., Eckhardt, S., Tapia, C., Vargas, A., Yasunari, T.J., 2012. Xenon-133 and caesium-137 releases into the atmosphere from the Fukushima Dai-ichi nuclear power plant: determination of the source term, atmospheric dispersion, and deposition. Atmos. Chem. Phys. 12 (5), 2313–2343.
Straume, A.G., Dietz, R.N., Koffi, E.N.d., Nodop, K., 1998. Perfluorocarbon background concentrations in Europe. Atmos. Environ. 32 (24), 4109–4122.
Tang, X., Zhu, J., Wang, Z.F., Gbaguidi, A., 2011. Improvement of ozone forecast over Beijing based on ensemble Kalman filter with simultaneous adjustment of initial conditions and emissions. Atmos. Chem. Phys. 11 (24), 12901–12916.
Tang, X., Zhu, J., Wang, Z.F., Wang, M., Gbaguidi, A., Li, J., Shao, M., Tang, G.Q., Ji, D.S., 2013. Inversion of CO emissions over Beijing and its surrounding areas with ensemble Kalman filter. Atmos. Environ. 81 (0), 676–686.
Ten Hoeve, J.E., Jacobson, M.Z., 2012. Worldwide health effects of the Fukushima Daiichi nuclear accident. Energy Environ. Sci. 5 (9), 8743–8757.
Van dop, H., et al., 1998. ETEX: a European tracer experiment; observations, dispersion modelling and emergency response. Atmos. Environ. 32 (24), 4089–4094.
Winiarek, V., Bocquet, M., Saunier, O., Mathieu, A., 2012. Estimation of errors in the inverse modeling of accidental release of atmospheric pollutant: application to the reconstruction of the cesium-137 and iodine-131 source terms from the Fukushima Daiichi power plant. J. Geophys. Res.-Atmos. 117.
Winiarek, V., Bocquet, M., Duhanyan, N., Roustan, Y., Saunier, O., Mathieu, A., 2014. Estimation of the caesium-137 source term from the Fukushima Daiichi nuclear power plant using a consistent joint assimilation of air concentration and deposition observations. Atmos. Environ. 82, 268–279.
Yasunari, T.J., Stohl, A., Hayano, R.S., Burkhart, J.F., Eckhardt, S., Yasunari, T., 2011. Cesium-137 deposition and contamination of Japanese soils due to the Fukushima nuclear accident. Proc. Natl. Acad. Sci. 108 (49), 19530–19534.
Yoshida, N., Kanda, J., 2012. Tracking the fukushima radionuclides. Science 336 (6085), 1115–1116.
Zhang, X.L., Chen, J.G., Su, G.F., Yuan, H.Y., 2013. Study on source inversion technology for nuclear accidents based on Gaussian Puff model and EnKF. In: Comes, T., Fiedrich, F., Fortier, S., Geldermann, J., Müller, T. (Eds.), The 10th International ISCRAM Conference, pp. 634–639. Baden-Baden, Germany.
Zhang, X.L., Su, G.F., Yuan, H.Y., Chen, J.G., Huang, Q.Y., 2014. Modified ensemble Kalman filter for nuclear accident atmospheric dispersion: prediction improved and source estimated. J. Hazard. Mater. 280 (0), 143–155.
Zheng, D.Q., Leung, J.K.C., Lee, B.Y., Lam, H.Y., 2007. Data assimilation in the atmospheric dispersion model for nuclear accident assessments. Atmos. Environ. 41 (11), 2438–2446.
Zheng, D.Q., Leung, J.K.C., Lee, B.Y., 2009. Online update of model state and parameters of a Monte Carlo atmospheric dispersion model by using ensemble Kalman filter. Atmos. Environ. 43 (12), 2005–2011.
Zheng, D.Q., Leung, J.K.C., Lee, B.Y., 2010. An ensemble Kalman filter for atmospheric data assimilation: application to wind tunnel data. Atmos. Environ. 44 (13), 1699–1705.